Wavelength-Dependent Roughness: A Quantitative Approach to Characterizing the Topography of Rough Titanium Surfaces

Marco Wieland, PhD[1]/Marcus Textor, PhD[2]/Nicholas D. Spencer, PhD[3]/Donald M. Brunette, PhD[4]

Topographies of grit-blasted, etched, grit-blasted and etched, and microfabricated and etched surfaces of commercially pure titanium have been investigated. Such surface topographies vary across the scale range of interest for dental implants, extending from nanometers to millimeters. The complete characterization of topography requires the use of complementary methods. This study compared the topographic characterization methods of non-contact laser profilometry, interference microscopy, stereo-scanning electron microscopy (stereo-SEM), and atomic force microscopy. Non-contact laser profilometry was shown to be a useful method to characterize topographic features in the micron to millimeter range, whereas interference microscopy and stereo-SEM can be employed down to the submicron range. Stereo-SEM is particularly useful for quantifying topographies with complex, strongly corrugated ("sharp"), and high-aspect-ratio features and was shown to be complementary to non-contact laser profilometry and interference microscopy. Because of tip-related envelope problems, atomic force microscopy was not found to be suitable for the type of surfaces investigated in this study. Independent of the method used, the commonly used "integral" amplitude roughness parameters, such as R_a, R_q, or R_t, were often of limited value in the description of actual implant surfaces. The application of the wavelength-dependent roughness approach was shown to be an effective method for the description of surface topographies in the complete range of characteristic roughness and is also a useful means of examining the effects of surface treatment processes. (Int J Oral Maxillofac Implants 2001;16:163–181)

Key words: *atomic force microscopy, dental implants, interference microscopy, non-contact laser profilometry, stereo-SEM, surface properties*

The chemical and topographic properties of implant surfaces are believed to be major factors in determining the interaction of implants with the biological environment, because these properties influence the formation of the foreign material/tissue interface and thereby the long-term success or failure of tissue integration.[1–3] Typical dental implant surfaces include topographic features in the millimeter to the nanometer range that are all believed to be relevant to the biological response of the host.[3]

The effects of surface topography on cell adhesion vary with the type of cell. More human gingival fibroblasts attach to electropolished surfaces than to etched or blasted surfaces.[4] In contrast, osteoblast-like cells demonstrate significantly higher levels of cell attachment to rough surfaces than to smooth surfaces.[5] Furthermore, studies in cell culture have demonstrated that the geometric dimensions of microstructured surface features, as well as their orientation, influence cell adhesion, morphology, orientation, proliferation, differentiation, and production of local factors.[6–10]

Of particular interest are studies examining the behavior of osteoblastic cells on commercially pure

[1]Postdoctoral Research Fellow, Faculty of Dentistry, Department of Oral Biological and Medical Sciences, University of British Columbia, Vancouver, British Columbia, Canada; and Laboratory for Surface Science and Technology, Department of Materials, Swiss Federal Institute of Technology, Zürich, Switzerland.
[2]Lecturer and Senior Scientist, Laboratory for Surface Science and Technology, Department of Materials, Swiss Federal Institute of Technology, Zürich, Switzerland.
[3]Professor, Laboratory for Surface Science and Technology, Department of Materials, Swiss Federal Institute of Technology, Zürich, Switzerland.
[4]Professor and Associate Dean of Research, Faculty of Dentistry, Department of Oral Biological and Medical Sciences, University of British Columbia, Vancouver, British Columbia, Canada.

Reprint requests: Prof Dr N. D. Spencer, Laboratory for Surface Science and Technology, NO H64, Department of Materials, ETH Zürich, Sonneggstrasse 5, CH-8092 Zürich, Switzerland. Fax: +41 1 633 1027. E-mail: nspencer@surface.mat.ethz.ch

titanium (cpTi) that have demonstrated that proliferation decreases with increasing surface roughness, whereas differentiation increases.[11–14] In vivo, surface topography has been found to influence the evolution and properties of the implant-tissue interface such as the degree of foreign body response and the percentage of new bonelike tissue close to the implant surface.[15] Surface roughening of dental implants has either been achieved adventitiously during the fabrication process or by subsequent treatment, and the processes involved include machining, particle-blasting, titanium plasma-spraying, chemical/electrochemical etching, or particle-blasting and chemical etching. Such treated dental and hip joint implants have been found in experimental studies to promote bone integration and long-term stability of implants.[15–24] Surface roughness has also been reported to determine the shear strength of the implant-bone interface—important for long-term fixation.[16,19,20,23] Given the importance of surface roughness on implant performance, it appears important to employ appropriate and precise methods to characterize rough surface topographies.

A large number of 2-dimensional (2-D) and 3-dimensional (3-D) measurement techniques are available to characterize surface topography, including the mechanical stylus, non-contact laser profilometry (LPM), interference microscopy (IM), confocal laser-scanning microscopy (CLSM), scanning tunneling microscopy (STM), and atomic force microscopy (AFM).[25–28] All measuring systems have vertical and lateral limitations in terms of measuring range and resolution.[25–27] These limitations are related to the physical basis of the methods; that is, the "true" surface topography, with information about surface wavelengths from zero to infinity, will never be obtained.[27] Furthermore, the problem of distortion of the true surface[25–28] (eg, envelope effects[26,29]) and the surface deformation[30] are issues in mechanical contact mode techniques such as AFM and the mechanical stylus. Optical artifacts are problematic in optical instruments such as LPM, IM, or CLSM because of microgeometry, inclination, and reflectivity of the surface.[28,31] Although 3-D roughness values have recently been introduced[28,32] and data published for dental implants,[15,33] the problem of accurately characterizing surfaces is further compounded by the lack of appropriate standards for 3-D surface roughness measurements.[34]

In most investigations, surface topographies are either characterized qualitatively using scanning electron microscopy (SEM) or one of the characterization techniques listed above, and data are presented in the form of numeric standard ("integral") surface roughness parameters, such as R_a, R_{max}, or R_t.[11,12,14,17,19] These parameters provide information about feature height, but they are often of limited value in describing more complex surfaces.[25–28,35] An adequate description of surface roughness requires parameters that quantify amplitude, spacing, and hybrid information[15,25–28,33,35] (Table 1). Only a few studies in the biomaterials field, however, have included spacing parameters[16,20,36–39] or both spacing and hybrid parameters[15,33,35] in addition to amplitude parameters.

The topographic features of commercially available dental implants vary widely.[15,33] The work of Buser and associates[17] and Cochran and coworkers[24] suggests that, at least for dental implants under experimental conditions, surfaces with an average roughness R_a of 3 μm to 4 μm provide excellent substrates for this purpose. In contrast, Wennerberg[15] found that an R_a of about 1.5 μm with an average spacing of 11.1 μm and an area ratio (effective area/geometric area) of 1.5 gave the firmest bone fixation among the surface structures tested. The differences in these conclusions could result from the variety in design and topography of the different implant systems used. Another problem, however, is that different methods (mechanical stylus versus CLSM) with different resolutions were used to describe the topographies. Also, the measured scan length and area were different.

There is a general problem in the characterization of surface topographies with conventional, "integral" roughness parameter sets, because these parameters are scale-dependent[26,27,40]; that is, the values will depend on the measurement scale and the sampling interval. Sayles and Thomas[40] demonstrated that the square of the standard deviation of the height distribution, σ^2, or R_q^2, of a profile is proportional to the measured distance along the surface. Moreover, the roughness values depend on the cutoff wavelength applied,[25,33,35,41] which separates roughness from waviness and form before calculating roughness.[25] Therefore, roughness values have to be presented together with their scan lengths or areas and information about the chosen cutoff filter. Furthermore, "integral" roughness parameters are of very limited value in describing the complex surface structures present on surface-treated titanium implants,[35] because the fine surface roughness features in the low micron or nanometer range, which may be important for interaction of the surface with adsorbed cellular entities and proteins, are often hidden by the coarser contributions to roughness and cannot be separated by calculations in accordance with standards such as DIN 4768[42] and DIN 4777.[43] Moreover, 2 technical surfaces with entirely different topographies and behaving very differently in a

Table 1 Definition of Selected Standard ("Integral") 2-D Roughness Parameters with Respect to Amplitude, Spacing, or Combined Amplitude and Spacing Characteristics

Roughness parameters	Definition	Type*	Description
R_a (µm)	$R_a = \frac{1}{m}\sum_{i=1}^{m}\lvert z(x_i)\rvert$	A	The arithmetic average of the absolute values of all points of the profile; also called CLA (center line average height)
R_q (µm)	$R_q = \sqrt{\frac{1}{m}\sum_{i=1}^{m} z^2(x_i)}$	A	The root mean square (RMS) of the values of all points of the profile
R_t (µm)		A	The maximum peak-to-valley height of the entire measurement trace
R_{zDIN} (µm)	$R_{zDIN} = \frac{1}{5}\sum_{i=1}^{5} z(x_i)$	A	The arithmetic average of the maximum peak to valley height of the roughness values $z(x_1)$ to $z(x_5)$ of 5 consecutive sampling sections over the filtered profile
S_m (mm)	$S_m = \frac{1}{m}\sum_{i=1}^{m} S_i$	S	Arithmetic average spacing between the falling flanks of peaks on the mean line
S_k	$S_k = \frac{1}{n}\sum_{i=1}^{n}\frac{y_i^3}{R_q^3}$	H	Amplitude distribution skew $S_k = 0$: amplitude distribution is symmetric $S_k < 0$: profile with "plateaus" and single-deep valleys $S_k > 0$: profile with very intense peaks
L_r	$L_r = \frac{L_0}{L_m}$	H	The relationship of the stretched length of the profile L_0 to the scanned length L_m

*A = amplitude; S = spacing; H = hybrid parameter (combined amplitude and spacing).

given biological situation may have the same R_a and R_q values. One approach to overcome these disadvantages is to calculate "differential" scale-dependent roughness functions using the wavelength-dependent roughness method to replace the "integral" roughness values with "window-related" parameters describing the various contributions to roughness in different dimensional ranges.[35,41] This method also enables the comparison of surface roughness values obtained with different instruments in the same wavelength range.[35]

The present study focused on comparison of the topographic surface analysis methods LPM, IM, stereo-SEM, and AFM, using both common "integral" roughness parameters and wavelength-dependent roughness evaluation. The window roughness parameters were calculated in predefined wavelength ranges. Grit-blasted, etched, grit-blasted and etched, and microfabricated and etched surfaces were investigated to illustrate the effect on commercially pure titanium (cpTi) surfaces of consecutive surface-structuring processes. The grit-blasted and etched surface closely resembles one that has been recently developed for the SLA-ITI dental implant (Straumann, Waldenburg, Switzerland), which appears to be particularly effective for bone integration and stability.[17,19,20,23,24]

MATERIALS AND METHODS

Materials

Commercially pure titanium (cpTi) surfaces were investigated in the form of discs 15 mm in diameter and 1 mm in thickness. A stamping procedure was used to produce the Ti discs out of a grade 2 cpTi sheet (ASTM F67) in an annealed condition, followed by 1 of 4 surface treatment protocols:

1. Grit-blasting with alumina beads under industrial particle-blasting conditions (average particle size: 250 µm).
2. Acid-etching in a hot solution of hydrochloric acid/sulfuric acid (HCl/H_2SO_4).
3. Grit-blasting with alumina beads under industrial particle-blasting conditions (average particle size: 250 µm) and etching in a hot solution of HCl/H_2SO_4.

Table 2 Advantages and Limitations of the Techniques Used in this Study to Characterize Surface Topographies

Method (environment)	Advantages	Limitations
Non-contact laser profilometry (air)	Non-contact, non-destructive Fast for 2-D profiles (minutes) Resolution: vertical about 50 nm, lateral about 1 µm Scanning over mm to cm possible	Artifacts (optical effects at sharp edges, reflections at locally shiny areas) Time-consuming for 3-D images (h)
Interference microscopy (air)	Non-contact, non-destructive Fast (3-D images, minutes) Resolution: vertical about 1 nm, lateral about 0.2 µm	Only small area measured at high lateral resolution For larger areas, adjacent images with high resolution have to be combined
Scanning electron microscopy (high vacuum)	High resolution: vertical 1 nm, lateral 10 nm High depth of focus Morphologic information Local chemical analysis (electron dispersive spectroscopy)	No quantitative topographic information
Stereo-scanning electron microscopy (high vacuum)	High depth of focus High dynamic x,y,z-range (mm to nm) Resolution: vertical 0.5 µm to 0.1 µm, lateral 20 nm to 50 nm Quantitative topographic information (2-D)	Not widely used Unsuitable for smooth surfaces Only small area at high lateral resolution For larger areas, adjacent micrographs with high resolution have to be combined
Atomic force microscopy (air, liquid, vacuum)	Highest resolution in both lateral and vertical directions (atomic to nm)	Limited z-range (problems with rough surfaces) Artifacts (envelope effect because of tip shape, surface deformation), particularly for high-aspect-ratio surfaces

4. Microfabrication by photolithography and electrochemical micromachining in a 3 mmol/L H_2SO_4/methanol electrolyte using a negative polyimide-based photoresist (Waycoat HNR 80, Olin Hunt, Norwalk, CT),[44] followed by etching in a hot solution of HCl/H_2SO_4. Before etching, the microfabricated surface is characterized by a regular array of hemispherical pits with diameters of 30 µm and depth of 15 µm.

Methods

Four different methods—LPM, IM, stereo-SEM, and AFM—were used to characterize the topographies of the grit-blasted, etched, grit-blasted and etched, and microfabricated and etched surfaces. Table 2 summarizes the surface characterization methods used, together with their advantages and limitations.

Non-Contact Laser Profilometry. Two-dimensional profiles and 3-D surface topographies were determined with a non-contact laser profilometer (UBM Messtechnik, Ettlingen, Germany), using a Microfocus sensor based on an autofocusing system. It operates with an optical head incorporating a 780-nm wavelength semiconductor laser, yielding a measurement spot size of about 1 µm. The nominal lateral and vertical resolutions of the system are 1 µm and 50 nm, respectively. Two-dimensional profiles were randomly obtained over a distance of 4.096 mm with a lateral resolution of 1,000 measurement points/mm. Area measurements were done over a 150 ×150-µm square and resolution in x- and y-directions of 1 µm and 2 µm, respectively. Laser profilometry is limited to lateral topographic features of ≥ 2 µm size.

Interference Microscopy. Three-dimensional surface topographies were determined by optical interference microscopy using a WYKO NT 2000 white-light interference microscope (Veeco Instruments, Tucson, AZ) based on phase shifting and vertical scanning interferometry. The WYKO NT 2000 system is equipped with a Michelson interferometer and objectives with magnifications of ×5, ×10, and ×50. The nominal lateral and vertical resolutions are 1.5 µm to 0.2 µm and 1 nm, respectively. Area measurements were done over 94.3×124.0 µm. To characterize larger areas of the different surfaces using IM, adjacent images were combined. In these instances, the measured areas were 282.9×372.0 µm.

Stereo-Scanning Electron Microscopy. Scanning electron microscopy (Philips XL30, FEI Company, Eindhoven, The Netherlands) was applied to all surfaces at 20 keV accelerating voltage. The advantages of SEM include a large depth of focus, high lateral resolution down to the nm range, the feasibility to

study structures with high aspect ratio, and direct production of images of the surfaces. Micrographs produced by SEM easily give a 3-D impression of the surface. However, quantitative topographic information cannot be obtained from a single micrograph. Therefore, viable non-destructive techniques for extracting surface microtopography from SEM micrographs were developed.[45–48] In this study, reconstruction of the stereo-SEM micrographs and computation of the height profiles, both based on the work of Desai,[49] were obtained using the analySIS Pro software (Version 2.11, SOFT Imaging System, Münster, Germany). Stereoscopic pairs of micrographs were obtained by tilting the object by –3 degrees (left image) and +3 degrees (right image) out of the initial position at 2 magnifications of ×1,000 and ×2,000 (lateral resolution of 0.064 µm and 0.032 µm, respectively). Because the direction of the tilt axis is parallel to the micrograph, the tilt can only yield horizontal shifts X_{sh} between the position of a point on the first and the second micrograph expressed by the parallax P. A simple relationship exists between the height h of any point and its X-shift X_{sh}:

$$h = \frac{X_{sh} \times X_{sc}}{2\sin(\omega/2)} \qquad \text{(Equation 1)}$$

$$X_{sh} = \frac{P}{\cos(\omega/2)} \qquad \text{(Equation 1a)}$$

For Equations 1 and 1a, X_{sc} = X-scale of the micrograph and ω = total tilt angle. This approach yields only 2-D profiles. In this study, profile lengths of 130 µm and 65 µm were computed. Such profiles, however, can be obtained comprehensively over an area by scanning and 3-D characterization.

Atomic Force Microscopy. Atomic force microscopy (Nanoscope E, Digital Instruments, Santa Barbara, CA) was used to measure the topographies of all investigated surfaces. Area measurements were done using the standard contact mode over a 144.4×144.4 µm square with a scan rate of 2 Hz.

Roughness Calculation Procedures. "Integral" Roughness Calculation. Before "integral" roughness parameters can be calculated, the waviness has to be separated by a phase-correct filtering in accordance with standards such as DIN 4768.[42] The cutoff wavelength, λ_c, is used to separate the roughness, waviness, and form of a profile or an area. To correctly compare surface roughness values obtained with different instruments, it must be ensured that the same filter and cutoff wavelength apply to the profiles and areas for all roughness calculations, independent of the instrument used.[34] Furthermore, the same software must be used to eliminate "software effects."[35] In practice, the cutoff is chosen by the instrument with the largest working area, which in this study was the LPM. If a smaller cutoff is used, part of the roughness may be lost. Therefore, in this study a Gaussian filter and an attenuation factor of 50% at the cutoff wavelength, λ_c, of 0.58 mm were applied to the LPM profiles using the software provided with the LPM (UBM version 1.5). After that, the roughness parameters were calculated within the UBM software. For stereo-SEM and IM, profiles were exported and read in by the UBM software, and the same calculation procedures as described above were applied to the data.

Wavelength-Dependent Roughness Evaluation. In metrology, it is well known that many types of surfaces used in engineering practice have random features, including form, roughness, and waviness. Two characteristics are needed to define completely such surface topographies: one related to the roughness height distribution or amplitude of the waveform and the other related to the spacing or wavelength.[50,51] The power spectra and the autocorrelation function give information related to wavelength and height distribution of the surface, whether periodic or random, and that allows form, roughness, and waviness to be separated from each other.[25–27,50,51] Both functions are based on the Fourier transform and are scale-dependent. Other scale-dependent functions are the cutoff filtering in the form of an infinitely sharp cutoff, RC (resistor capacity), or Gaussian filter,[25,26,50,51] which are used in surface metrology for separating the waviness and form from the roughness of the surface. Fractal analysis is another method used to characterize surface topographies. The essential difference between fractal analysis and other approaches is that fractal analysis describes a surface with the fractal dimension[52]—a single scale-independent parameter.

The concept of the wavelength-dependent evaluation procedure applied in this paper differs from commonly used procedures in the sense that it treats the low-wavelength (λ_l) and high-wavelength (λ_h) cutoffs as variable parameters. Therefore, it is a scale-dependent evaluation. Details of the evaluation based on the relationship between the Fourier coefficients A_n and B_n and the roughness parameter R_q have been discussed earlier.[35,41] The data points of obtained profiles or areas are limited according to the resolution and measuring range of the method used. Therefore, the roughness defined as R_q^2 corresponds to the sum of the squared Fast

Fourier Transformation (FFT) coefficients in the corresponding range *l* to *h*:

$$R_q^2(l,h) = \frac{A_0^2}{2} + \frac{1}{2}\sum_{n=l}^{n=h} A_n^2 + B_n^2 \quad \text{or approximately}$$

$$R_q^2(l,h) = \frac{1}{2}\sum_{n=l}^{n=h} A_n^2 + B_n^2 \qquad \text{(Equation 2)}$$

since the term $\frac{A_0^2}{2}$ is generally negligible.

Equation 2 is defined as "window roughness," where *l* and *h* are the range of the Fourier coefficients, corresponding to the range of wavelengths and defining a certain "window" to be chosen according to application-oriented considerations.[35,41] The lowest meaningful value *l* is, according to the Nyquist theorem,[25] twice the lateral distance between experimental points; the highest meaningful value *h* is 0.2 times the scan length.

The concept of scale-dependent roughness has 2 main advantages. First, it allows one to calculate roughness values within different preset wavelength ranges. The window can therefore be chosen according to the specific situation under consideration. The second advantage is that it enables one to compare data of the same surface determined by different techniques, or of different surfaces determined with the same technique.[35] In such a situation it must be ensured that the different measurements are evaluated using the same low- and high-frequency cutoff.

The wavelength-dependent roughness evaluation using FFT was performed within the software program Maple (Version Maple V, Release 5). First, the raw z(x) profiles obtained by the LPM are filtered using the UBM software to separate the waviness according to DIN 4768[42] using a Gaussian cutoff filter (λ_c = 0.58 mm) with an attenuation factor of 50% and then exported as an ASCII file and read in by Maple. After that, the FFT of each profile is calculated. In the next step, the upper cutoff wavelength (λ_h) is steadily decreased from 0.2 times the profile length to 2 times the step size of adjacent data points, while the lower resolution length (λ_l) is fixed at 2 times the resolution limit of the particular characterization technique used.[35,41] After each decreasing step, R_q^2 is calculated according to equation 2, and finally the square root of R_q^2 is determined. The result demonstrates the dependence of the roughness R_q on the profile wavelength, λ ($R_q = f(\lambda)$; see Results). For window-roughness calculations of a particular window of interest, both the low- and the high-wavelength cutoff are set accordingly.[35,41] The back-transformed real profile is again imported in the UBM software, where the window-roughness parameters in the chosen scale range are calculated. Also, 2-D profiles or 3-D areas may be shown, which correspond to the selected wavelength (or scale) ranges (see Results).

In the case of the computed stereo-SEM profiles and the IM profiles, profiles were first exported and read in by the UBM software to separate the waviness. Then the profiles were again exported and read in by Maple, and the same procedures as described above for the LPM profiles were applied to the stereo-SEM and IM data.

Statistics

Different roughness parameters obtained from the "integral" as well as window roughness calculations were tested for statistical significance using Bonferroni in a 1-way analysis of variance. That is, values of each roughness parameter calculated from the profiles obtained from each method were averaged to give the mean. After that, pairwise multiple comparisons were used to test the differences between each pair of means of a given roughness parameter at a level of $P < .05$.

RESULTS

To compare the topographic surface analytic methods of LPM, IM, and stereo-SEM, the same area of the grit-blasted and etched surface, as well as of the microfabricated and etched surface, was investigated. The microfabricated and etched surface, produced by a precise microfabrication technique and subsequent etching process, had pits of 30 µm diameter and 15 µm depth before etching. Figures 1a to 1f show the surface topographies of the grit-blasted and etched as well as the microfabricated and etched sample obtained by SEM, IM, and LPM. Scanning electron micrographs (Figs 1a and 1b) show topographic features such as edges and pits more clearly and give a better 3-D impression than the IM or LPM images (Figs 1c and 1d and 1e and 1f, respectively). However, IM and LPM images can easily be viewed computationally as 3-D plots. In the case of SEM, the method of stereo-imaging can be used. Figures 2a to 2c show the reconstructed stereo-SEM micrograph of the microfabricated and etched surface (Fig 2a) as well as the corresponding 3-D plots of the IM and LPM images (Figs 2b and 2c).

The SEM micrograph (Fig 1a) and especially the stereo-SEM micrograph (Fig 3) of the grit-blasted and etched surface clearly demonstrate 2 topographic contributions, one in the range of 20 to 40 µm (primarily produced by the alumina-blasting

Figs 1a to 1f The same areas of a grit-blasted and etched surface and of a microfabricated and etched surface were investigated using scanning electron microscopy, interference microscopy, and non-contact laser profilometry. In particular, the SEM micrographs show surfaces with 2 different, superimposed surface topographies.

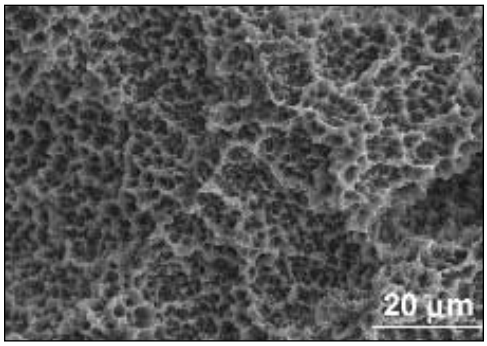

Fig 1a Grit-blasted and etched surface investigated using SEM.

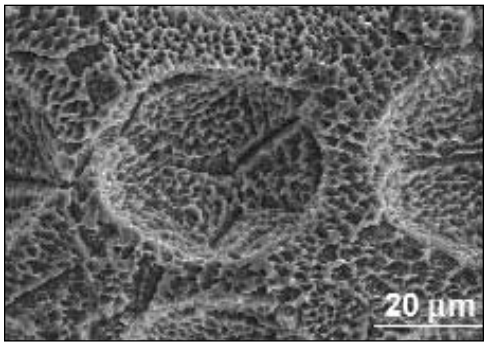

Fig 1b Microfabricated and etched surface investigated using SEM.

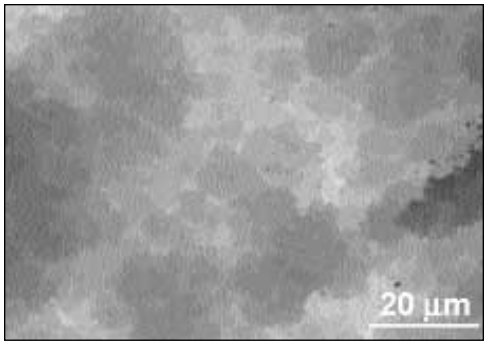

Fig 1c Interference microscopic examination of grit-blasted and etched surface.

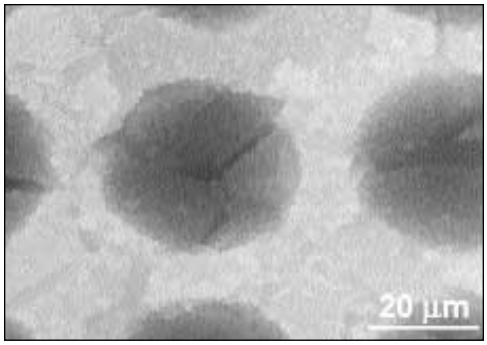

Fig 1d Interference microscopic examination of microfabricated and etched surface.

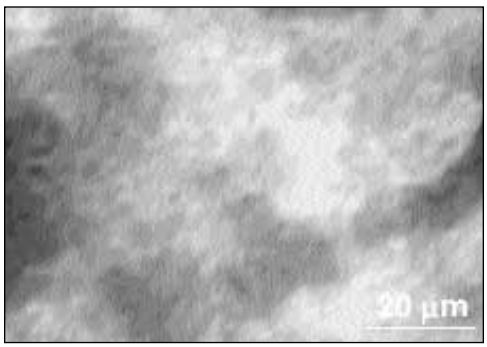

Fig 1e Non-contact laser profilometric examination of grit-blasted and etched surface.

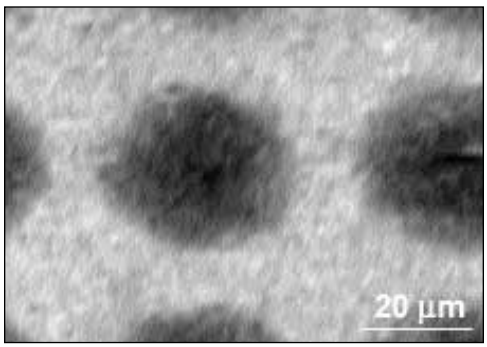

Fig 1f Non-contact laser profilometric examination of microfabricated and etched surface.

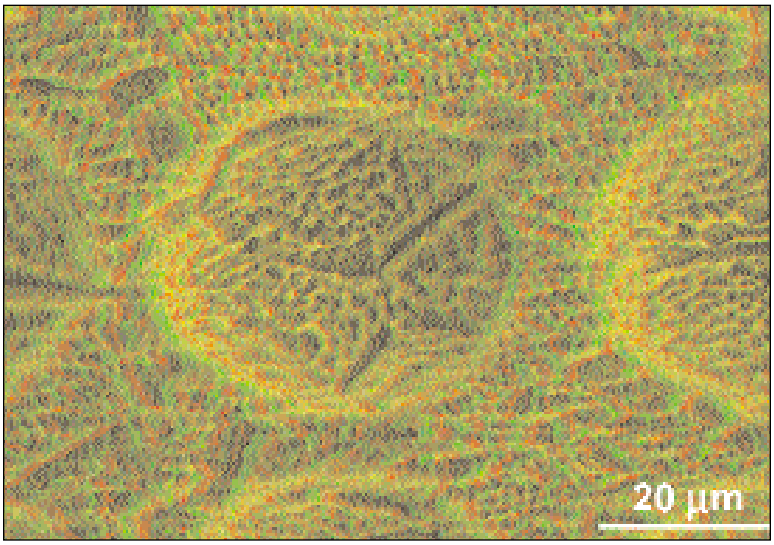

Fig 2a Reconstructed stereo-SEM micrograph of the microfabricated and etched surface. An optical stereo-effect can be achieved by using a red *(left eye)*/green *(right eye)* pair of glasses.

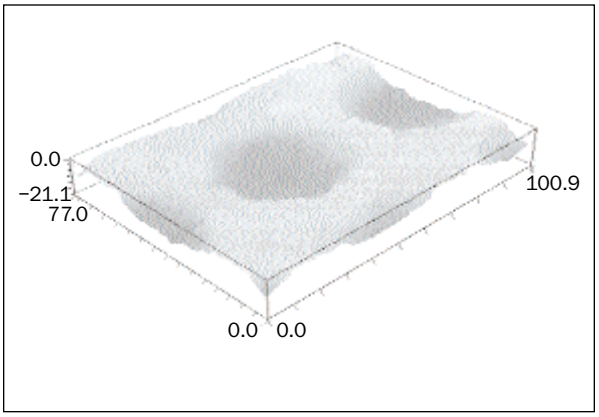

Fig 2b Corresponding 3-D plot of the IM image (all measurements in µm).

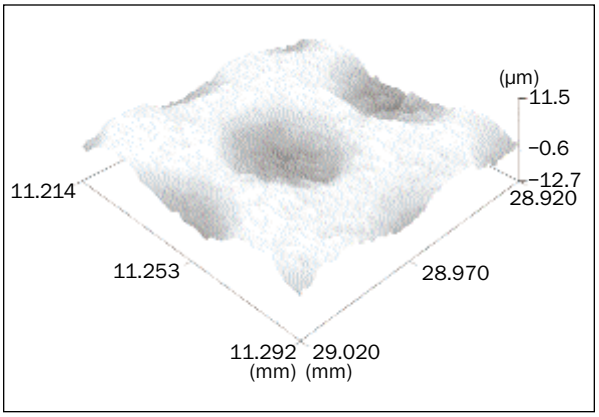

Fig 2c Corresponding 3-D plot of the LPM image.

process and subsequent removal of the particles by the chemical etching process), and the other in the range of about 0.5 to 2 µm (produced by the chemical etching process). In the case of the microfabricated and etched surface, both the SEM and the stereo-SEM micrograph (Figs 1b and 2a) also demonstrate 2 topographic contributions, one from the pits (30 µm in diameter, 15 µm in height) and the other again in the range of about 0.5 to 2 µm (produced by the chemical etching process).

Atomic force microscopic studies showed that the grit-blasted and etched and the microfabricated and etched surfaces had height distributions that were too large for accurate use of the technique. For example, Fig 4 shows an AFM scan of the grit-blasted and etched surface over an area of 141.6×141.6 µm square. The true surface is strongly distorted because of limitations in the z-direction and tip envelope effects. Therefore, no AFM studies were performed on such surfaces.

"Integral" Roughness Calculation

For the quantitative description of the surfaces shown in Figs 1a to 1f, 7 profiles of the grit-blasted and etched surface were selected parallel to the x-direction of the 3-D data set determined with LPM and IM. Furthermore, 7 profiles were computed from the reconstructed stereo-SEM micrograph. To describe the pattern of the microfabricated and etched surface, a profile was selected along the

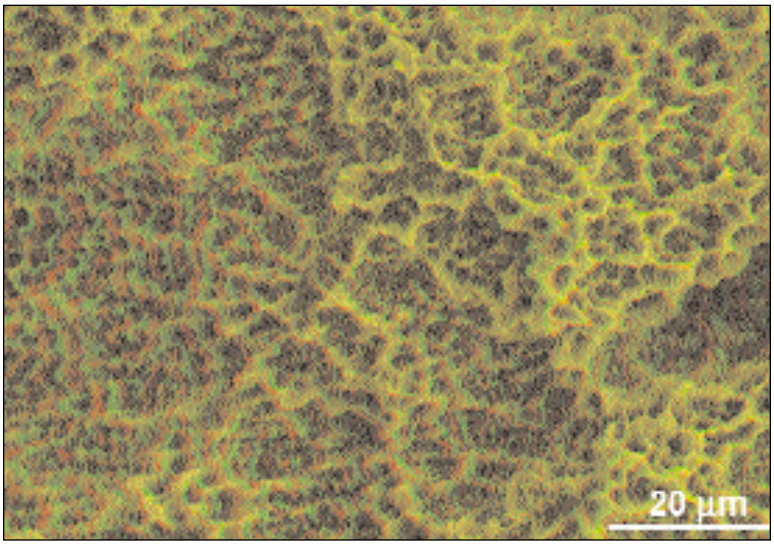

Fig 3 The grit-blasting and etching processes of the grit-blasted and etched surface result in a topography with 2 characteristic contributions in the ranges of 0.5 to 2 µm and 20 to 40 µm as shown in this stereo-SEM micrograph. An optical stereo-effect can be achieved by using a red *(left eye)*/green *(right eye)* pair of glasses.

diameter of the pit, and the roughness parameters R_t and S_m were calculated. Table 3 summarizes the results of the "integral" roughness evaluation using the UBM software. The selected profile length was, in all cases, 85 µm. In the case of the grit-blasted and etched surface, the R_a, R_q, R_t, R_{zDIN}, S_m, S_k, and L_r values (see Table 1) were chosen to represent amplitude, spacing, and hybrid parameters.[15,25–28,33,35,41]

The microfabricated and etched surface was used as a reference surface. The heights and diameters of the pits of this surface, expressed by the roughness parameters R_t and S_m, were calculated for the profiles obtained from the 3 methods. The results for R_t (between 14.93 µm and 18.84 µm) and S_m (between 32 µm and 34 µm) were in the expected ranges, given by the height (15 µm) and diameter (30 µm) of the pits before etching. The conclusion is that IM as well as stereo-SEM can be used in addition to LPM to characterize surface topographies in that range. However, the topographic features produced by the subsequent etching could not be separately characterized.

In the case of the grit-blasted and etched surface, the results show that the L_r value differed significantly ($P < .05$) between the measurement methods IM and stereo-SEM, as well as between LPM and stereo-SEM. L_r was lower in the cases of LPM and IM, which can be explained by the lower resolution of these methods (lateral resolution of 1 µm for LPM and 0.2 µm for IM) and the "smoothing" of the true profile in comparison with the stereo-SEM technique (lateral resolution of about 0.064 µm under the chosen condition). To illustrate these effects, a part of the same profile of the grit-blasted and etched surface was selected from the 3-D data set of the LPM and IM measurements as well as from the computed profile of the stereo-SEM micrograph (Figs 5a to 5c).

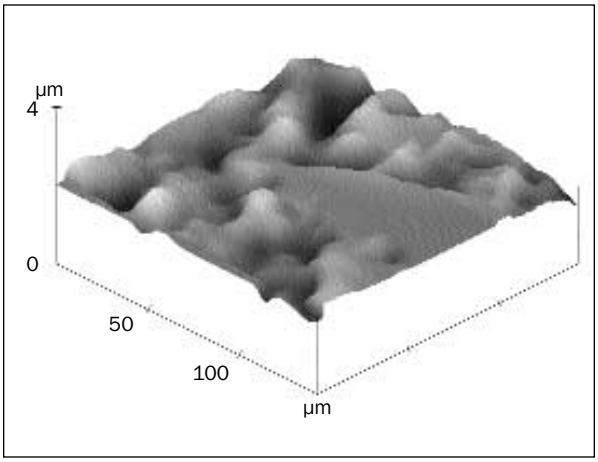

Fig 4 Atomic force microscopic image of the grit-blasted and etched surface. The height distribution of that surface is too large for AFM studies. Some parts of the surface were too deep to be measured.

No other significant differences could be found for all other calculated "integral" roughness parameters. However, there was a tendency toward higher values for the amplitude parameters R_a, R_q, and R_{zDIN} in the following order: calculated from stereo-SEM profiles < IM profiles < LPM profiles (Table 3). This observation is likely to be related to optical artifacts of the laser (LPM) and light (IM) reflection at sharp topographic discontinuities.[25,28] In the case of the mean groove distance S_m, one would expect from Figs 1a and 3 that S_m would be much smaller for the stereo-SEM profiles because of the fact that SEM is able to resolve the fine etch structure (in the range of 0.5 to 2 µm), in contrast to LPM and IM. However, there are 2 major problems: *(1)* In the case of the

Table 3 Roughness Values Calculated from LPM, IM, and Stereo-SEM Profiles

	Grit-blasted and etched surface			Microfabricated and etched surface		
Roughness parameters	**LPM profiles**	**IM profiles**	**Stereo-SEM profiles**	**LPM profiles**	**IM profiles**	**Stereo-SEM profiles**
R_a (µm)	3.93 ± 0.93	3.41 ± 0.78	3.10 ± 2.06	—	—	—
R_q (µm)	4.69 ± 1.19	4.08 ± 0.99	3.71 ± 2.13	—	—	—
R_t (µm)	15.00 ± 2.11	12.41 ± 1.72	12.76 ± 4.1	18.84	15.51	14.93
R_{zDIN} (µm)	6.83 ± 0.82	6.62 ± 1.50	5.89 ± 1.17	—	—	—
S_m (mm)	0.027 ± 0.005	0.031 ± 0.007	0.021 ± 0.008	0.032	0.034	0.032
S_k	0.14 ± 0.09	–0.13 ± 0.44	0.03 ± 0.15	—	—	—
L_r	1.81 ± 0.14	1.52 ± 0.10	2.57 ± 0.55	—	—	—

Selected from 3-D data sets or computed from stereo-SEM micrographs shown in Figs 1 to 3. All calculations were performed with UBM software using a Gaussian filter with an attenuation factor of 50% at the cut-off wavelength λ_c = 0.58 mm (n = 7 for the grit-blasted and etched surface [means ± SD]; n = 1 for the microfabricated and etched surface).

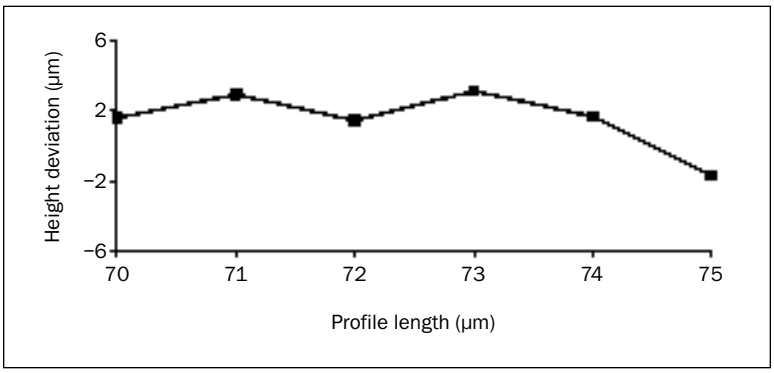

Fig 5a Parts of the 2-D profile of the grit-blasted and etched surface selected from the 3-D LPM data set.

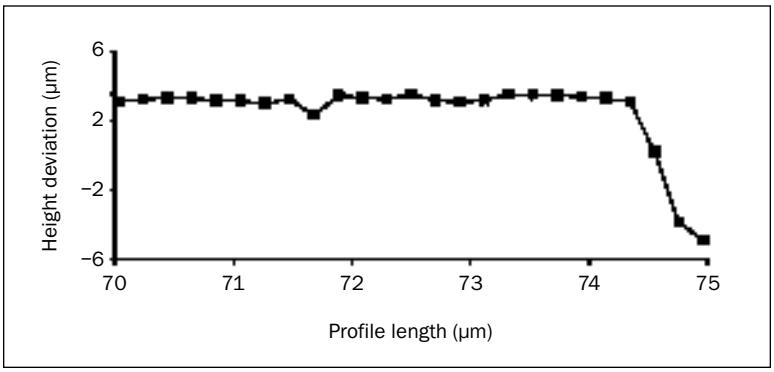

Fig 5b Parts of the same 2-D profile selected from the 3-D IM data set.

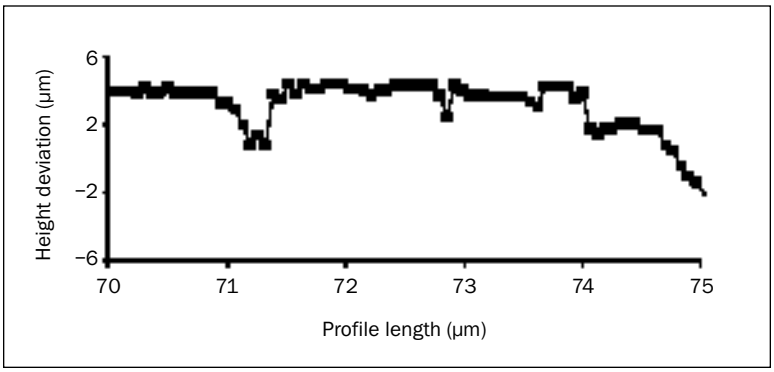

Fig 5c Parts of the same 2-D profile selected from the computed stereo-SEM micrograph.

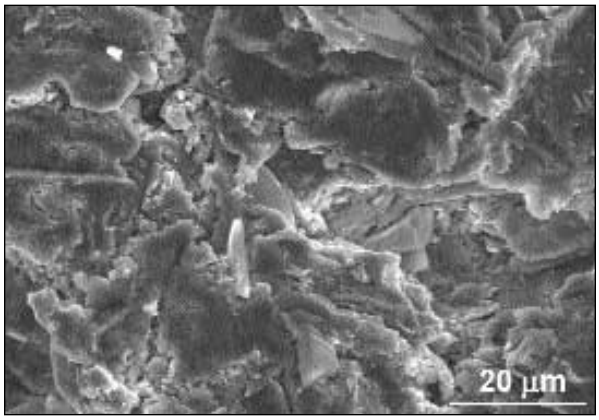

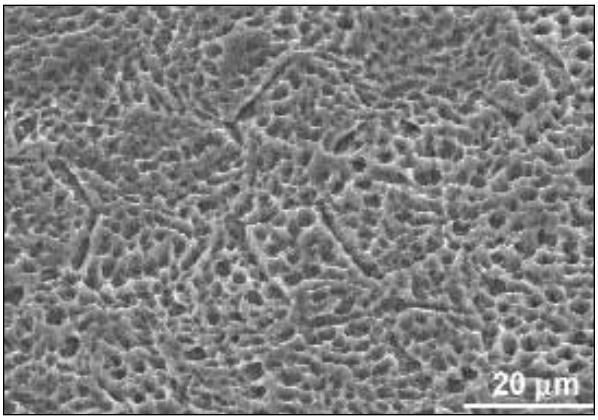

Figs 6a and 6b Scanning electron micrographs of *(left)* the grit-blasted and *(right)* the etched surfaces.

stereo-SEM profiles, small features of the fine etch structure are filtered out when calculating the spacing parameter according to a norm such as DIN 4768, with the consequence that S_m reflects only the spacing of the grit-blasted surface structure (which is resolved by all experimental techniques); and *(2)* In the case of LPM and IM, there is insufficient resolution to determine the small features.

Regardless of the instrument used, the smaller topographic contribution in the range of 0.5 to 2 µm (produced by the etching step) could not be sufficiently characterized with the "integral" roughness parameters for both the grit-blasted and etched and the microfabricated and etched surface, although the lateral resolution of stereo-SEM and the vertical resolution of all methods were high enough to resolve these features. Therefore, another procedure must be used for the characterization of surface topographies. In the next section, the wavelength-dependent roughness evaluation will be proposed as a possible method to characterize small surface features independent of the rougher contributions.

Wavelength-Dependent Roughness Evaluation

To obtain more specific information on the effect of each treatment step, grit-blasted, etched, and grit-blasted and etched titanium surfaces were investigated. Seven 2-D profiles of each surface type were obtained with LPM, IM, and stereo-SEM. The measured profile lengths were 4.096 mm (LPM), 372 µm (IM), and 130 µm and 65 µm (stereo-SEM). The corresponding SEM micrographs are shown in Figs 1a and 6.

Figure 7 presents a comparison of wavelength-dependent roughness evaluations of the grit-blasted and etched surface obtained with LPM, IM, and stereo-SEM. According to Equation 2 (see Roughness Calculation Procedures), the highest $R_q(\lambda)$ value for each curve $R_q = f(\lambda)$, which is the averaged curve of the 7 measured profiles, includes all calculated wavelengths of the profiles and corresponds to the "integral" R_q value. Decreasing the upper wavelength limit results in a decreased R_q (λ) value. However, in the case of LPM, the curve $R_q = f(\lambda)$ was constant up to the cutoff wavelength of 0.58 mm. Above 0.58 mm, the curve shows no additional contribution to the roughness, because these features were filtered out by the previous separation of waviness and roughness with the Gaussian filter at the cutoff wavelength of 0.58 mm. Below 0.58 mm, the curve decreases, with a decreasing upper wavelength limit. Between a wavelength of about 40 µm and 4 µm, the curves $R_q = f(\lambda)$ of the LPM and IM profiles are congruent. That means that in this range, the 2 techniques provide similar data. The curves of the IM profiles and the stereo-SEM profiles cross each other at a wavelength of about 1 µm. Above 1 µm, the curve of the stereo-SEM profiles shows slightly but consistently lower wavelength-dependent $R_q(\lambda)$ values compared to IM and LPM. The different physical principles of detection and possible artifacts are probable reasons for this difference. However, the stereo-SEM curve is sufficiently similar to the others to justify combining all 3 curves to reflect the whole range. For each curve, the roughness values drop dramatically at twice the lateral resolution limits of the methods, whether instrumental (LPM and IM) or acquisitional (stereo-SEM). According to Nyquist's theorem,[25] the lowest wavelength that can be defined corresponds to twice

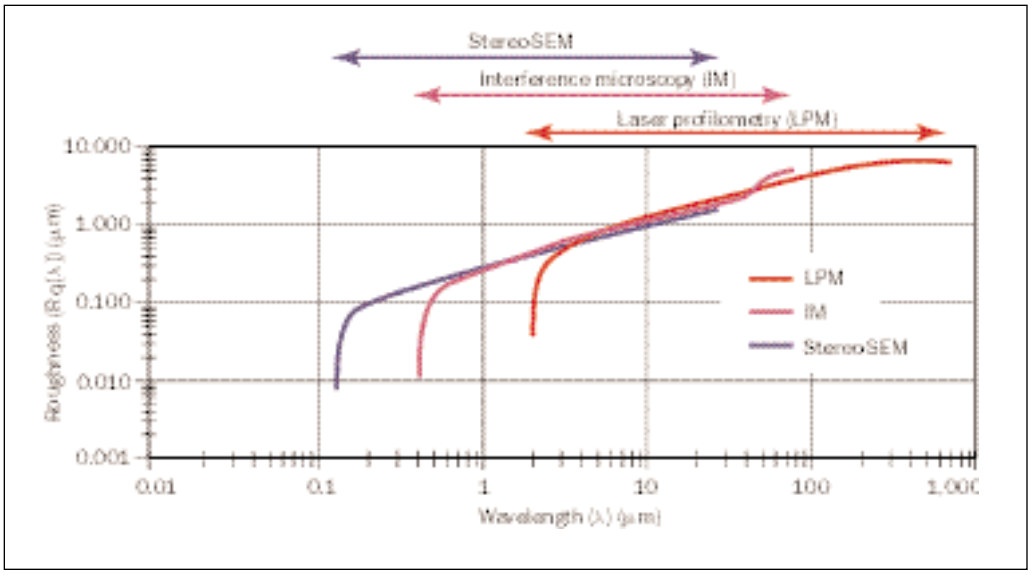

Fig 7 Comparison of the wavelength-dependent roughness evaluations of the grit-blasted and etched surface using 7 profiles measured with LPM, IM, and stereo-SEM.

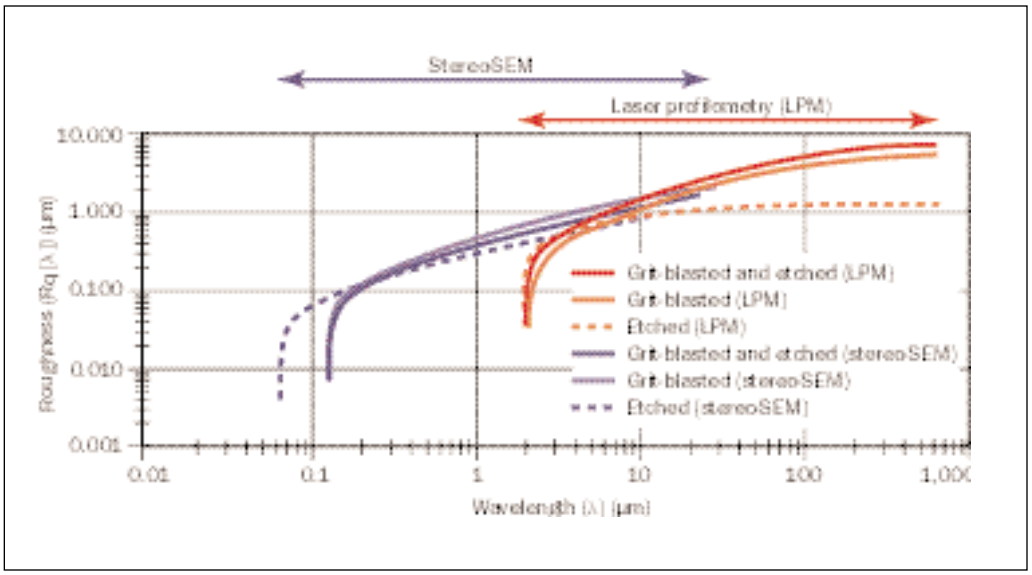

Fig 8 Comparison of the dependence of the roughness $R_q(\lambda)$ on the profile wavelength for etched, grit-blasted, and grit-blasted and etched surfaces using 7 profiles of each type of surface measured with LPM and stereo-SEM.

the lateral resolution. The resolution of the SEM profiles can be improved using a higher magnification to resolve smaller features as shown in Fig 8 for the etched surface.

Figures 1a and 3 demonstrate that the grit-blasted and etched surface has 2 superimposed topographies in different scale ranges: one resultant to the grit-blasting process (20 to 40 µm) and a second, 1 to 2 orders of magnitude finer (0.5 to 2 µm), that is related to the etching process. Specific information about each treatment step is given in Fig 8, which shows the averaged curves $R_q = f(\lambda)$ of the grit-blasted, etched, and grit-blasted and etched surfaces, each calculated from 7 LPM and stereo-SEM

profiles. For all 3 curves $R_q = f(\lambda)$ calculated from the LPM profiles, the $R_q(\lambda)$ values are constant up to the cutoff wavelength of 0.58 mm. These $R_q(\lambda)$ values correspond to the "integral" R_q values. Below the cutoff wavelength of 0.58 mm, the curves steadily decrease with decreasing upper wavelength limit. The resolution limit of the LPM is again evident at the wavelength of 2 μm, as discussed above (see also Fig 7). The curve of the grit-blasted and etched surface crosses the curve of the grit-blasted surface twice at wavelengths of 65 μm and 7.4 μm, respectively. The wavelength-dependent roughness within that window (65 μm and 7.4 μm) shows lower $R_q(\lambda)$ values for the grit-blasted and etched surface compared to the grit-blasted surface. The probable explanation is that the etching process removed the alumina beads left over from the grit-blasting process and smoothed the sharp edges of the surface at the same time.

For the grit-blasted surface data obtained with stereo-SEM, the curve $R_q = f(\lambda)$ decreases with decreasing upper wavelength limit and starts at the wavelength of 26 μm with a higher value than the grit-blasted and etched surface. A similar result was found in this range for the 2 curves calculated from the LPM profiles. Between wavelengths of 10 μm and 4 μm, the curves for the 2 surfaces are congruent. Below 4 μm, the wavelength-dependent roughness demonstrates lower $R_q(\lambda)$ values with decreasing upper wavelength limit for the grit-blasted and etched surface compared to the grit-blasted surface. In the case of the etched surface description obtained by stereo-SEM, the curve starts at a wavelength of 13 μm with a smaller $R_q(\lambda)$ value as computed from the LPM profiles. Below 4 μm the curves of the grit-blasted and etched surface and the etched surface are congruent.

These data indicate that in the range below 4 μm, only the effects of the etching process are evident on the etched and the grit-blasted and etched surfaces. Furthermore, the results of the wavelength-dependent roughness evaluation demonstrate the dependence on magnification of the resolution limit of the stereo-SEM data. The etched surface was determined with a magnification of ×2,000, whereas the magnification used on the grit-blasted and grit-blasted and etched surfaces was ×1,000. Therefore, the curve of the etched surface dramatically drops off at a lower wavelength than the other 2 curves. These results demonstrate that the wavelength-dependent roughness evaluation is limited only by the resolution of the instrument used and its limited measuring range or by the acquisition conditions. If the resolution of the instrument were in the atomic range (AFM) or in the nanometer range (high-resolution SEM), topographic features in the range of a few nanometers could be characterized as well.

Another application of the wavelength-dependent roughness evaluation is the calculation of window roughness. In this method, the roughness $R_q(\lambda)$ for each surface in the various scale ranges of interest is calculated. For example, one could calculate roughness separately in the topographic ranges produced by grit-blasting (20 to 40 μm) and chemical etching (0.5 to 2 μm). It is also possible to calculate additional amplitude and spacing as well as hybrid parameters in the different wavelength ranges of interest. To perform this calculation, the measured or computed profiles have first to be FFT transformed and then inverse transformed with iFFT into specific wavelength ranges of interest, as discussed earlier. The results are window-specific, scale- or wavelength-dependent profiles, from which roughness parameters can then be calculated. An example is given for the grit-blasted and etched surface. The same 7 profiles obtained with LPM, IM, and stereo-SEM were used for the window roughness calculation, as used above for the wavelength-dependent roughness curve ($R_q = f(\lambda)$) evaluation. The roughness parameters were calculated with the UBM software as described earlier. Table 4 lists the roughness parameters R_a, R_q, R_t, R_{zDIN}, S_m, S_k, and L_r calculated for the different windows 0.4 to 3 μm, 3 to 10 μm, 10 to 50 μm (in the case of stereo-SEM: 10 to 26 μm), and 50 to 500 μm and for the original full-scale profiles. The roughness values shown are meaningful considering the resolution of the techniques and the finite measuring length. Figures 9a to 9d show part of one original IM profile together with its iFFT-filtered profiles in the wavelength ranges 0.4 to 3 μm, 3 to 10 μm, and 10 to 50 μm.

The roughness values calculated from the original profiles correspond to the "integral" roughness values. However, the values for the original IM and stereo-SEM profiles are shown in parentheses, because they correspond to profiles taken along very short distances of 372 μm and 130 μm, respectively, and reflect the "total roughness" across the limited scale ranges of 0.4 μm to 74.4 μm and 0.12 μm to 26.0 μm, respectively. Because of this limited range, the amplitude parameters are correspondingly lower by a factor of 2 to 3 in comparison to the LPM profiles; the latter were taken over a distance of 4.096 mm that also included the important range of 50 μm to 500 μm.

The roughness values calculated for the different windows indicated that the amplitude parameters R_a, R_q, R_t, and R_{zDIN} and the spacing parameter S_m systematically decreased as the window range was

Table 4 Roughness Values Calculated from LPM, IM, and Stereo-SEM Profiles of the Grit-Blasted and Etched Surface

Method	Roughness parameters	Roughness values (ranges) 0.4 to 3 µm	3 to 10 µm	10 to 50 µm*	50 to 500 µm	Original profiles†
LPM	R_a (µm)	—	0.98 ± 0.02	2.01 ± 0.22	4.47 ± 0.39	5.09 ± 0.39
	R_q (µm)	—	1.25 ± 0.02	2.56 ± 0.28	5.66 ± 0.45	6.40 ± 0.50
	R_t (µm)	—	9.29 ± 0.62	18.42 ± 4.38	31.90 ± 3.52	40.28 ± 5.43
	R_{zDIN} (µm)	—	8.06 ± 0.14	14.17 ± 2.27	23.25 ± 1.97	31.18 ± 2.87
	S_m (mm)	—	0.006 ± 0.000	0.028 ± 0.003	0.127 ± 0.018	0.030 ± 0.003
	S_k	—	0.07 ± 0.05	0.06 ± 0.14	–0.11 ± 0.35	–0.06 ± 0.20
	L_r	—	1.71 ± 0.01	1.18 ± 0.02	1.05 ± 0.01	1.81 ± 0.01
IM	R_a (µm)	0.15 ± 0.02	0.86 ± 0.10	2.68 ± 0.94	—	(4.61 ± 1.08)
	R_q (µm)	0.26 ± 0.07	1.19 ± 0.20	3.33 ± 1.13	—	(5.76 ± 1.45)
	R_t (µm)	6.22 ± 3.26	12.16 ± 6.51	15.78 ± 5.25	—	(25.34 ± 6.08)
	R_{zDIN} (µm)	2.89 ± 0.83	7.09 ± 1.68	11.29 ± 3.06	—	(16.60 ± 3.35)
	S_m (mm)	0.001 ± 0.000	0.005 ± 0.001	0.029 ± 0.004	—	(0.022 ± 0.005)
	S_k	–0.02 ± 0.18	0.20 ± 0.10	–0.13 ± 0.41	—	(–0.22 ± 0.25)
	L_r	1.70 ± 0.13	1.87 ± 0.15	1.22 ± 0.08	—	(2.06 ± 0.12)
Stereo-SEM	R_a (µm)	0.14 ± 0.02	0.76 ± 0.01	1.84 ± 0.46	—	(2.44 ± 0.63)
	R_q (µm)	0.22 ± 0.06	0.97 ± 0.02	2.31 ± 0.59	—	(3.17 ± 0.92)
	R_t (µm)	3.59 ± 2.22	7.43 ± 0.51	10.65 ± 3.06	—	(18.76 ± 5.34)
	R_{zDIN} (µm)	2.14 ± 1.05	5.01 ± 0.13	6.92 ± 1.59	—	(10.87 ± 1.48)
	S_m (mm)	0.001 ± 0.000	0.005 ± 0.000	0.029 ± 0.002	—	(0.013 ± 0.005)
	S_k	–0.14 ± 0.24	0.08 ± 0.27	0.14 ± 0.46	—	(–0.20 ± 0.37)
	L_r	1.84 ± 0.19	1.66 ± 0.05	1.12 ± 0.04	—	(2.32 ± 0.28)

The values are given for the original profiles and the 4 different wavelength ranges 500 to 50 µm, 50 to 10 µm, 10 to 3 µm, and 3 to 0.4 µm, respectively. All calculations were performed with UBM software using a Gaussian filter and an attenuation factor of 50% at the cutoff wavelength of 0.58 mm. n = 7 for each surface; mean values ± standard deviations shown.
*For stereo-SEM, a range of 10 to 26 µm was used.
†Parentheses for IM and stereo-SEM indicate profiles taken along very short distances of 372 µm and 130 µm, respectively, and reflect the "total roughness" across the limited scale ranges.

shifted to smaller dimensions. This is because ever-decreasing dimensions of height and spacing were evaluated in this procedure. The hybrid parameter L_r, on the other hand, increased when the window was moved to smaller dimensions, because smaller dimensions more effectively contribute to the increase in specific length than coarser dimensions.

Another advantage of the wavelength-dependent roughness concept is the visualization of the topographies in selected wavelength ranges by digital processing using iFFT filters in the desired ranges. Figures 10a to 10d show the original SEM micrograph together with the iFFT-filtered SEM micrographs in the 3 selected wavelength ranges 50 to 10 µm, 10 to 3 µm, and 3 to 0.4 µm. The filtered SEM micrographs allow visual judgment of the effects of different surface treatments separately, eg, of the alumina blasting and etching process in the case of the grit-blasted and etched surface.

DISCUSSION

The same area of a grit-blasted and etched surface and a microfabricated and etched surface was investigated using LPM, IM, and stereo-SEM. The LPM method best measures the topographic features in the range of a few microns to millimeters, since this technique is limited to lateral topographic features larger than 2 µm. To extend the information to the submicron range, stereo-SEM micrographs and IM images were taken of the same surfaces and computationally transformed to quantitative line profiles. Interference microscopy has particular value in measuring topographic features in the range of 0.5 µm to 300 µm. Stereo-SEM is useful for quantifying topographies with complex, strongly corrugated ("sharp"), and high-aspect-ratio properties, with only a small risk of artifacts and "distortions" of the true profiles or areas in the range of around 50 nm

Figs 9a to 9d Part of original IM profile and its iFFT-filtered profiles of the grit-blasted and etched surface in different wavelength ranges. Wavelength-dependent roughness parameters are calculated from these profiles.

Fig 9a Original profile.

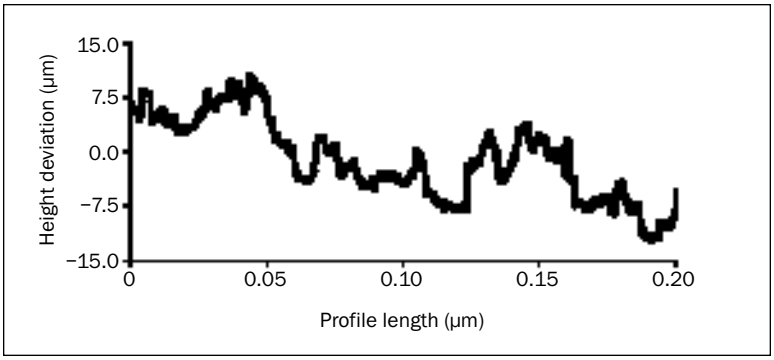

Fig 9b Profile filtered in wavelength range 50 to 10 µm.

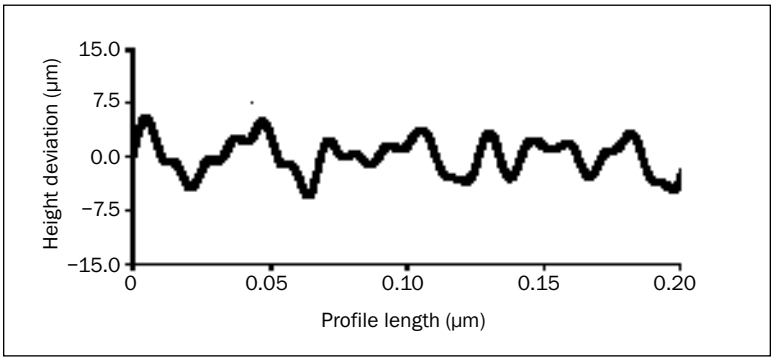

Fig 9c Profile filtered in wavelength range 10 to 3 µm.

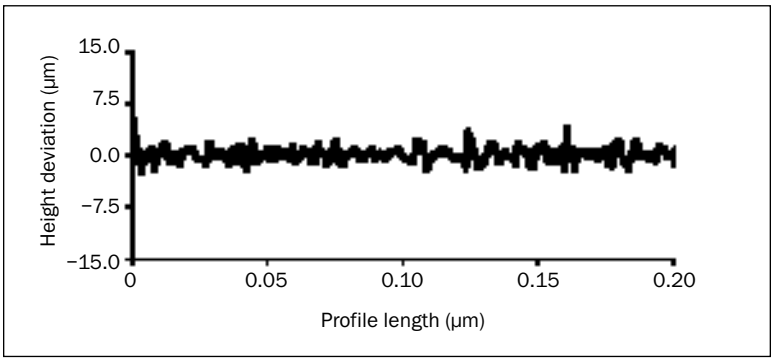

Fig 9d Profile filtered in wavelength range 3 to 0.4 µm.

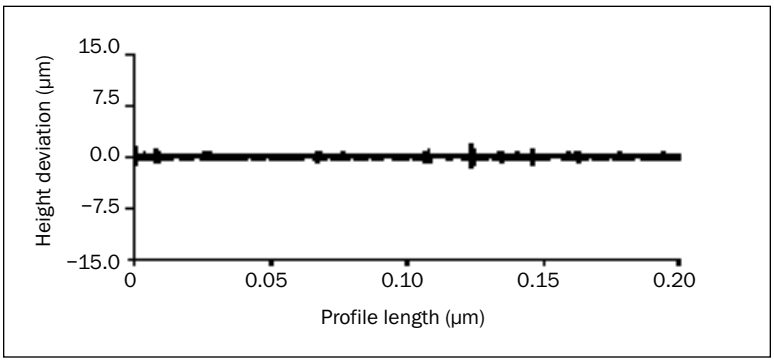

Figs 10a to 10d Scanning electron micrograph of the grit-blasted and etched surface, and iFFT-filtered surfaces based on the window roughness evaluation concept in different wavelength ranges to show topographic contributions of the different ranges.

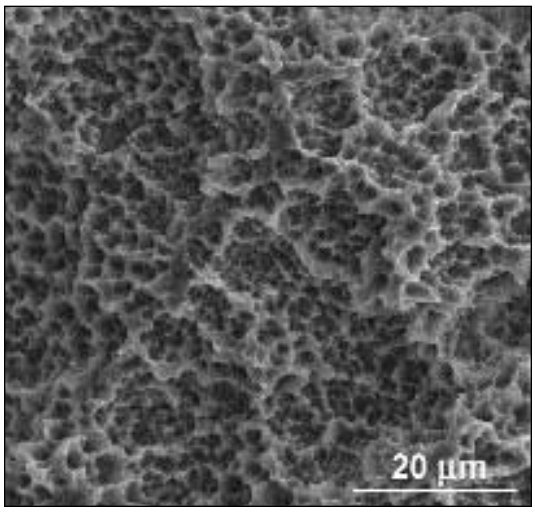

Fig 10a Original SEM micrograph of the grit-blasted and etched surface (Fig 1a).

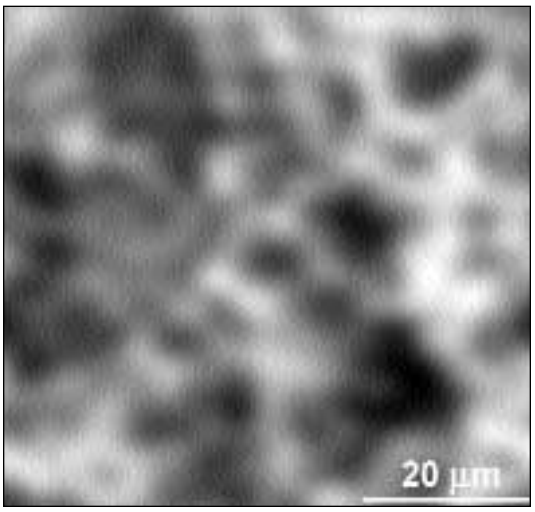

Fig 10b iFFT-filtered image in the wavelength range 50 to 10 µm.

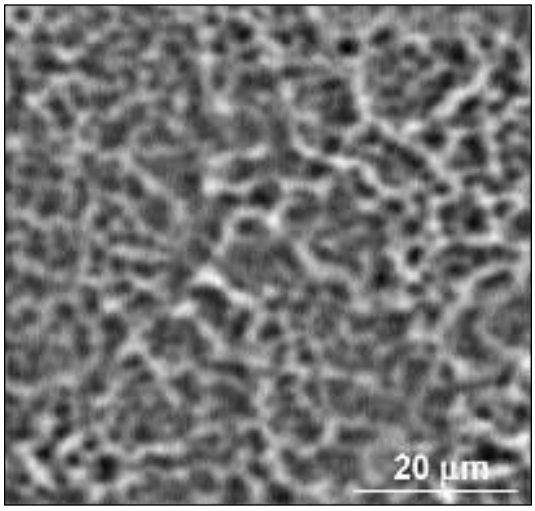

Fig 10c iFFT-filtered micrograph in the wavelength range 10 to 3 µm.

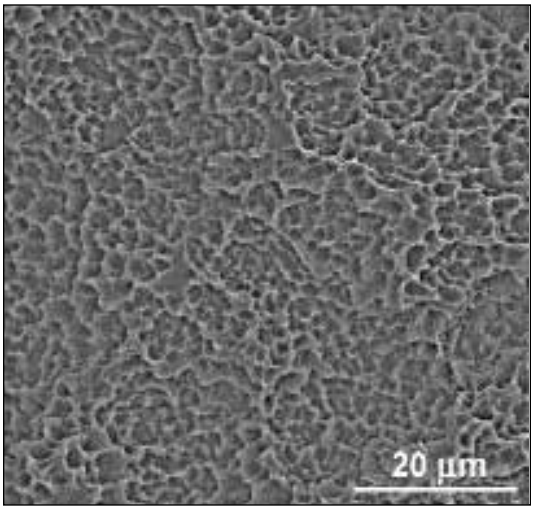

Fig 10d iFFT-filtered micrograph in the wavelength range 3 to 0.4 µm.

to 100 µm. The techniques LPM, IM, and stereo-SEM generally complement each other across a wide range of dimensions, as shown in the wavelength-dependent roughness studies.

A significant difference was found for the "integral" hybrid roughness value L_r between the techniques LPM and stereo-SEM, as well as between IM and stereo-SEM (see Table 3). However, there were no other significant differences for any other calculated "integral" roughness parameter between the 3 techniques measuring the same profiles. This lack of difference may partly be the result of relatively high standard deviations of the measurements, which are a consequence of the short scan length of 85 µm used in this study. A full description of the surface was not possible with this relatively short scan length, because some parts of form, waviness, and roughness could not be detected and therefore were lost. For example, it is known that the amplitude value R_q is linearly related to the square root of the measured distance along the surface.[26] The short scan length is a practical limitation of the stereo-SEM and IM and results in smaller amplitude roughness values compared to those calculated from the original LPM profiles (see Table 4).

Furthermore, the results of the "integral" roughness calculation demonstrated that, independent of the method used, these roughness parameters are of limited value in describing the surface structures of 2 superimposed topographies of different scale ranges. For example, the grit-blasted and etched surface, which is used in ITI implants,[17,19,20,23,24] has one feature related to the grit-blasting process and a second feature, produced by etching, that is 1 to 2 orders of magnitude finer. Standard "integral" amplitude roughness parameters do not adequately describe this structure, as the fine roughness features are hidden by the coarser contributions to roughness, whereas for the spacing parameter S_m, there is a computational problem related to the definition of this parameter. The calculation of S_m is highly dependent on the threshold settings, with the consequence that small features of the fine-etch structure were filtered out when calculating S_m according to the norm.

Wavelength-dependent roughness evaluation is useful in describing surface topographies produced by 2 consecutive surface-structuring processes, because the contributions in different wavelength ranges can be separately calculated. Furthermore, the results indicate that more than one instrument is needed to characterize such a surface because of the lateral and vertical resolutions, as well as artifacts and limited measuring range of the methods. This study shows that LPM, IM, and stereo-SEM must be used to characterize the whole range of topographies present from the macro- to the nano-range. A wavelength-dependent roughness evaluation enables the comparison of the different instrumental methods in the same wavelength range. This is an extremely important issue in comparing different methods that is overlooked by far too many users of roughness measurement equipment.[34] Another advantage of the wavelength-dependent roughness concept is the visualization of iFFT-filtered profiles and images, as shown in Figs 9 and 10. Particular aspects of selected topographic features such as area, form, depth, and their statistical distribution, as well as information on homogeneity/heterogeneity and isotropy/anisotropy across the surface, may be quantitatively evaluated with the help of image analysis software.

CONCLUSION

An important question in implant-related therapies is, how does the topography of a surface influence the biological response? Topographic features in different size ranges would be expected to influence such processes as protein adsorption or cell adhesion. The complete characterization of complex surface topographies of commercial implants requires more than one method to describe the whole surface topography, from the macro- to the nano-range. The proposed description of roughness in discrete windows provides the opportunity to correlate in vitro and/or in vivo biological performance data with surface topographic data over various size ranges that are relevant to the interaction of the surface with biomolecules such as proteins, with cells, and with tissue. In addition, wavelength-dependent roughness evaluation is very valuable in surface quality assurance and may serve as a useful indicator of the quantitative effect of surface treatment processes. It is particularly valuable for describing separately and quantitatively the topographic outcome of each individual treatment step in multi-step surface fabrication procedures.[35]

ACKNOWLEDGMENTS

The authors would like to thank Dr D. Snétivy and Dr C. Sittig of Straumann Institute, Waldenburg, Switzerland, for support and supply of the materials; Prof D. Landolt and Dr Ch. Madore, EPFL, Département des Matériaux, Lausanne, Switzerland, for supply of the materials; Dr W. Hotz, Alusuisse Technology and Management, Neuhausen am Rheinfall, Switzerland, for support of the IM studies; and Dr M. Schneidereit, SOFT Imaging System, Münster, Germany, for the free use of the analySIS Pro software. This study was financially supported by the Swiss

Priority Program on Materials Research (Program of the Board of the Swiss Federal Institutes of Technology) and the Canadian Institutes of Health Research Grant MT 7617.

REFERENCES

1. Albrektsson T, Brånemark P-I, Hansson HA, Lindström J. Osseointegrated titanium implants. Requirements for ensuring a long-lasting, direct bone-to-implant anchorage in man. Acta Orthop Scand 1981;52:155–170.
2. Ratner BD. The surface characterization of biomedical materials: How finely can we resolve surface structure? In: Ratner BD (ed). Surface Characterization of Biomaterials. Amsterdam: Elsevier, 1988:13–36.
3. Kasemo B, Lausmaa J. Surface science aspects on inorganic biomaterials. CRC Crit Rev Biocomp 1986;2:335–380.
4. Könönen M, Hormia M, Kivilahti J, Hautaniemi J, Thesleff I. Effect of surface processing on the attachment, orientation, and proliferation of human gingival fibroblasts on titanium. J Biomed Mater Res 1992;26:1325–1341.
5. Bowers KT, Keller JC, Randolph BA, Wick DC, Michaels CM. Optimization of surface micromorphology for enhanced osteoblast responses in vitro. Int J Oral Maxillofac Implants 1992;7(3):302–310.
6. Brunette DM. The effect of implant surface topography on the behaviour of cells. Int J Oral Maxillofac Implants 1988; 3:231–246.
7. Brunette DM. The effect of surface topography on cell migration and adhesion. In: Ratner BD (ed). Surface Characterization of Biomaterials. Amsterdam: Elsevier, 1988: 203–217.
8. Brunette DM. Effects of surface topography of implant materials on cell behavior in vitro and in vivo. In: Hoch HC, Jelinski LW, Craighead HG (eds). Nanofabrication & Biosystems. Cambridge: Cambridge Univ Press, 1996: 335–355.
9. Den Braber ET, de Ruijter JE, Smits HTJ, Ginsel LA, von Recum AF, Jansen JA. Quantitative analysis of cell proliferation and orientation on substrata with uniform parallel surface micro-grooves. Biomaterials 1996;17:1093–1099.
10. Den Braber ET, de Ruijter JE, Ginsel LA, von Recum AF, Jansen JA. Quantitative analysis of fibroblast morphology on microgrooved surfaces with various groove and ridge dimensions. Biomaterials 1996;17:2037–2044.
11. Boyan BD, Batzer R, Kieswetter K, Liu Y, Cochran DL, Szmukler-Moncler S, et al. Titanium surface roughness alters responsiveness of MG63 osteoblast-like cells to 1α,25-$(OH)_2D_3$. J Biomed Mater Res 1998;39:77–85.
12. Martin JY, Schwartz Z, Hummert TW, Schraub DM, Simpson J, Lankford J, et al. Effect of titanium surface roughness on proliferation, differentiation, and protein synthesis of human osteoblast-like cells. J Biomed Mater Res 1995;29: 389–401.
13. Boyan BD, Hummert TW, Kieswetter K, Schraub D, Dean DD, Schwartz Z. Effect of titanium surface characteristics on chondrocytes and osteoblasts in vitro. Cells Mater 1995; 5(4):323–335.
14. Kieswetter K, Schwartz Z, Hummert TW, Cochran DL, Simpson J, Dean DD, Boyan BD. Surface roughness modulates the local production of growth factors and cytokines by osteoblast-like MG-63 cells. J Biomed Mater Res 1996;32: 55–63.
15. Wennerberg A. On Surface Roughness and Implant Incorporation [thesis]. Göteborg: Göteborg University, 1996.
16. Wong M, Eulenberger J, Schenk R, Hunziker E. Effect of surface topology on the osseointegration of implant materials in trabecular bone. J Biomed Mater Res 1995;29: 1567–1575.
17. Buser D, Schenk RK, Steinemann S, Fiorellini JP, Fox CH, Stich H. Influence of surface characteristics on bone integration of titanium implants. A histometric study in miniature pigs. J Biomed Mater Res 1991;25:889–902.
18. Schenk RK, Buser D. Osseointegration: A reality. Periodontology 2000 1998;17:22–35.
19. Wilke HJ, Claes L, Steinemann SG. The influence of various titanium surfaces on the interface shear strength between implants and bone. In: Heimke G, Soltész U, Lee AJC (eds). Advances in Biomaterials. Vol 9: Clinical implant materials. Amsterdam: Elsevier, 1990:309–314.
20. Buser D, Nydegger T, Oxland T, Cochran DL, Schenk RK, Hirt HP, et al. Interface shear strength of titanium implants with a sandblasted and acid-etched surface: A biomechanical study in the maxilla of miniature pigs. J Biomed Mater 1999; 45:75–83.
21. Brånemark P-I, Hansson BO, Adell R, Breine U, Lindström J, Hallén O, Öhman A. Osseointegrated implants in the treatment of the edentulous jaw. Scand J Plast Reconstr Surg 1977;11(suppl 16).
22. Semlitsch MF, Weber H, Streicher RM, Schön R. Joint replacement components made of hot-forged and surface-treated Ti-6Al-7Nb alloy. Biomaterials 1992;13(11):781–788.
23. Steinemann SG, Eulenberger J, Mäusli PA, Schroeder A. Adhesion of bone to titanium. In: Christel P, Meunier A, Lee AJC (eds). Biological and Biomechanical Performance of Biomaterials. Amsterdam: Elsevier, 1986:409–414.
24. Cochran DL, Nummikoski PV, Higginbottom FL, Hermann JS, Makins SR, Buser D. Evaluation of an endosseous titanium implant with a sandblasted and acid-etched surface in the canine mandible: Radiographic results. Clin Oral Implants Res 1996;7(3):240–252.
25. Whitehouse DJ (ed). Handbook of Surface Metrology. Bristol, Philadelphia: Institute of Physics, 1994.
26. Thomas TR (ed). Rough Surfaces. London, New York: Longman Press, 1982.
27. Bennett JM, Mattsson L (eds). Introduction to Surface Roughness and Scattering. Washington, DC: Optical Society of America, 1989.
28. Stout KJ (ed). Three-Dimensional Surface Topography: Measurement, Interpretation and Applications. A Survey and Bibliography. London: Penton Press, 1994.
29. Von Weingraber H. Suitability of the envelope line as a reference standard for measuring roughness. Microtecnic 1957; 11:6–17.
30. Brown CA, Savary G. Describing ground texture using contact profilometry and fractal analysis. Wear 1991;141: 211–226.
31. Windecker R. Optisches Autofokus-Profilometer. Technisches Messen 1993;60:267–270.
32. Stout KJ, Sullivan PJ, Dong WP, Mainsah E, Luo N, Mathia T, Zahouani H. The development of methods for the characterisation of roughness in three dimensions. European Community Contract No 3374/1/0/170/90/2. Birmingham: Univ of Birmingham, 1993.
33. Wennerberg A, Albrektsson T. Suggested guidelines for the topographic evaluation of implant surfaces. Int J Oral Maxillofac Implants 2000;15(3):331–344.
34. Mattsson L. Surface roughness and microtopography. In: Brune D, Hellborg R, Whitlow HJ, Hunderi O (eds). Surface Characterisation: A User's Sourcebook. Weinheim: Scandinavian Science, 1997:82–100.

35. Wieland M. Experimental Determination and Quantitative Evaluation of the Surface Composition and Topography of Medical Implant Surfaces and Their Influence on Osteoblastic Cell-Surface Interactions [thesis]. Zürich: Swiss Federal Institute of Technology, 1999.
36. Ungersböck A, Rahn B. Methods to characterize the surface roughness of metallic implants. J Mater Sci Mater Med 1994;5:434–440.
37. Carlsson L, Regnér L, Johannsson C, Gottlander M, Herberts P. Bone response to hydroxyapatite-coated and commercially pure titanium implants in the human arthritic knee. J Orthop Res 1994;12(2):274–285.
38. Sittig C, Wieland M, Vallotton PH, Textor M, Spencer ND. Surface characterization of implant materials c.p. Ti, TiAlNb and TiAlV after different pretreatments. J Mater Sci Mater Med 1999;10:35–46.
39. Wieland M, Sittig C, Textor M, Schenk V, Ha SW, Keller BA, et al. Surface composition and topography of titanium alloy implants. In: Olefjord I, Nyborg L, Briggs D (eds). ECASIA97: 7th European Conference on Applications of Surface and Interface Analysis, Göteborg, Sweden, June 16–20, 1997. Göteborg: Chalmers Univ of Göteborg, 1997:139–142.
40. Sayles RS, Thomas TR. Surface topography as a nonstationary random process. Nature 1978;271:431–434.
41. Wieland M, Hänggi P, Hotz W, Textor M, Keller BA, Spencer ND. Wavelength-dependent measurement and evaluation of surface topographies: Application of a new concept of window roughness and surface transfer function. Wear 2000;237(2):231–252.
42. DIN 4768. Determination of surface roughness values of the parameters R_a, R_z, R_{max} by means of electrical contact (stylus) instruments; Terminology, measuring conditions. Berlin: Beuth, 1990.
43. DIN 4777. Metrology of surfaces; Profile filters for electrical contact stylus instruments. Berlin: Beuth, 1990.
44. Madore C, Landolt D. Electrochemical micromachining of controlled topographies on titanium for biological applications. J Micromech Microeng 1997;7:270–275.
45. Boyde A. Quantitative photogrammetric analysis and qualitative stereoscopic analysis of SEM images. J Microscopy 1973;98:452–471.
46. Hudson B. The application of stereo-techniques to electron micrographs. J Microscopy 1973;98:396–401.
47. Ghosh SK. Electron microscopy: Systems and applications. In: Karara HM, Adams LP (eds). Non-Topographic Photogrammetry, ed 2. Falls Church: American Society for Photogrammetry and Remote Sensing, 1989:187–201.
48. Boyde A. Aspects of 3-D imaging, display and measurement in light and scanning electron microscopy. Inst Phys Conf Ser 1993;130:353–360.
49. Desai V. Untersuchung von dreidimensionalen Rekonstruktionsverfahren in der Rasterelektronenmikroskopie und Realisierung einer schnellen Simulation [thesis]. Münster: Westfälischen Wilhelms-Universität, 1989.
50. Whitehouse DJ, Archard JF. The properties of random surfaces of significance in their contact. Proc R Soc Lond A 1970;316:97–121.
51. Spragg RC, Whitehouse DJ. A new unified approach to surface metrology. Proc Inst Mech Eng 1970;185:697–707.
52. Mandelbrot BB (ed). The Fractal Geometry of Nature. San Francisco: Freeman, 1982.